

Kinetics and safety analysis of sulfide mineral self-heating

Part I. Effect of mineralogy

Abduljelil Iiyas · Kelly Hawboldt · Faisal Khan

NATAS2010 Conference Special Issue
© Akadémiai Kiadó, Budapest, Hungary 2011

Abstract Thermal methods of analysis such as DSC and TGA provide a powerful methodology for the study of solid reactions. This paper proposes an improved thermal analysis methodology for thermal stability and safety investigation of complex solid-state reactions. The proposed methodology is based on differential iso-conversional approach and involves peak separation and individual peak analysis for kinetic analysis and safety prediction. The proposed thermal analysis method was coupled with Mineral Libration Analysis (MLA) to investigate self-heating of sulfide mineral ores. The influence of sample's mineralogy on thermal degradation was examined and discussed. The information gained from the advanced kinetic analysis of DSC/TGA measurements were up-scaled for TMR and SADT determination. The described thermal analysis method provides not only an understanding of sulfide mineral self-heating, but also aids the design of effective mitigation measures for their adverse environmental and safety effects.

Keywords Kinetics · DSC · TGA · Thermal analysis · Thermal safety · TMR

Introduction

With safety issues associated with processing, storage, and transportation of sulfide mineral ores/concentrates due to their self-heating propensity in the presence of air, increasing emphasis is placed upon precise determination kinetics of this phenomenon to assess its risks and to design

mitigation measures. Thermal risks of runaway reactions, such as self-heating, are characterized by their severity in terms of adiabatic temperature rise (ΔT_{AD}) and probability in terms of time to maximum rate under adiabatic conditions.

In continuation of our research on sulfide mineral self-heating behavior [1, 2], we report in this paper thermal safety prediction of self-heating based on iso-conversional kinetic analysis of dynamic DSC measurements. Previous related research works have mostly focused on role of mineralogy on reaction mechanisms [3], kinetics [2], products [4] and thermal stability [5, 6]. The purpose of this paper is to investigate the role of sulfide ore mineralogical contents on self-heating behavior from thermal safety standpoint.

Experimental section

Thirteen (13) ore samples were received from the Reid Brook deposit, Vale Inco. The samples were screened for thermal stability in a DSC system (STAR^c series from Mettler Toledo). The DSC was calibrated with an indium and zinc standard following the instrument calibration guidelines. In the dynamic mode of operation, approximately 10 mg of each sample is subjected to temperature ramp at 1, 2, 4, and 8 °C min⁻¹ heating rates under isobaric conditions with air (10 m L min⁻¹) as the purge gas. The samples were initially screened in cost saving aluminum hermetic pans. However, selected samples were tested under isochoric conditions in a high-pressure gold pan supply by the Swiss Safety Institute. To insure that the observed DSC exotherm is mainly due to oxidation, a test is repeated at 8 °C min⁻¹ in nitrogen environment (not shown).

A. Iiyas (✉) · K. Hawboldt · F. Khan
Faculty of Engineering and Applied Science, Memorial
University of Newfoundland, St. John's, NL A1B 3X5, Canada
e-mail: ajliyas@me.com

Numerical tools

The advanced thermokinetic software package AKTS—Thermo-kinetics and Thermal Safety Software was used for this study. The software suite is based on differential iso-conversional techniques. Baseline subtraction is a major problem in kinetic analysis of DSC curve; however, the AKTS software tool is capable of performing baseline optimization simultaneously with thermo-kinetic parameters determination thus increasing the accuracy of estimated thermo-kinetic parameters.

Results and discussions

Accuracy and reproducibility

Figure 1 shows the processing procedure for representative DSC curves by the AKTS software. The as-obtained DSC curve (Fig. 1a) is slope corrected if necessary (Fig. 1b). Following this, spline baseline subtraction was performed to adjust for the baseline and allow asymmetric Gaussian type functions to be fitted to the peak of interest (Fig. 1c). This is a routine mathematical step allowing for efficient peak separations (Fig. 1d). It must be mentioned that this step is pre-kinetic step, i.e., does not constitute kinetic analysis; nonetheless, very important as it enables deconvolution of DSC curves resulting in more accurate subsequent kinetic analyses.

To insure reproducibility of data, each test was conducted at least two times. A representative reproducibility plot is depicted in Fig. 2. Lastly, TGA tests were performed for each sample under similar conduction to the DSC tests to insure that the obtained DSC thermal events

result from thermo-chemical changes rather than phase or other structural changes. An overlay of representative DSC/TGA plot is shown in Fig. 3.

As shown in Fig. 3, a peak in DSC curves is mirrored by a sloped decrease in the TGA plot. Typically, DSC peak pre-supposes an endothermic or exothermic event due to moisture liberation, desulfurization, and/or oxidative sulfur to sulfur dioxide [7] resulting in sample weight loss evident in the TGA curve. An accurate overlap of the independent tests in the DSC and the TGA, at different ramp rates, also confirms the reproducibility of the results.

DSC measurements for effect of mineralogy on sulfide ore oxidation

Thirteen (13) sulfide mineral ore samples were obtained from Reid Brook deposits, courtesy of Vale Inco. Table 1 depicts the depths at which the samples were logged as well as their field observations at the time of logging. As shown in Table 2, the samples are rich in pyrrhotite, pentlandite, chalcopyrite, cubanite, magnetite, pyrite, and violarite. However, the mineral groups of concern are primarily pyrrhotite, pentlandite, and chalcopyrite and/or their respective major elemental species (Fe, Ni and Cu), which tends to exhibit greater influence on self-heating of sulfide ores [6, 8]. Thus, the present study is focused on the effects of these mineral groups and/or species on self-heating.

Figure 4 shows the as-obtained DSC signals for the different sulfide mineral ores in an air environment, ramped at 8 K/min in an aluminum hermetic cell. As previously mentioned, this pan type was used only for screen purposes, subsequent tests were conducted on the high-pressure sealed crucibles, which is critical for data up-scaling for safety predictions. It is evident from Fig. 4

Fig. 1 Analysis of DSC curves **a** Raw data, **b** Spline integration **c** Fit of asymmetric Gaussian type signals, **d** Resulting peak separation

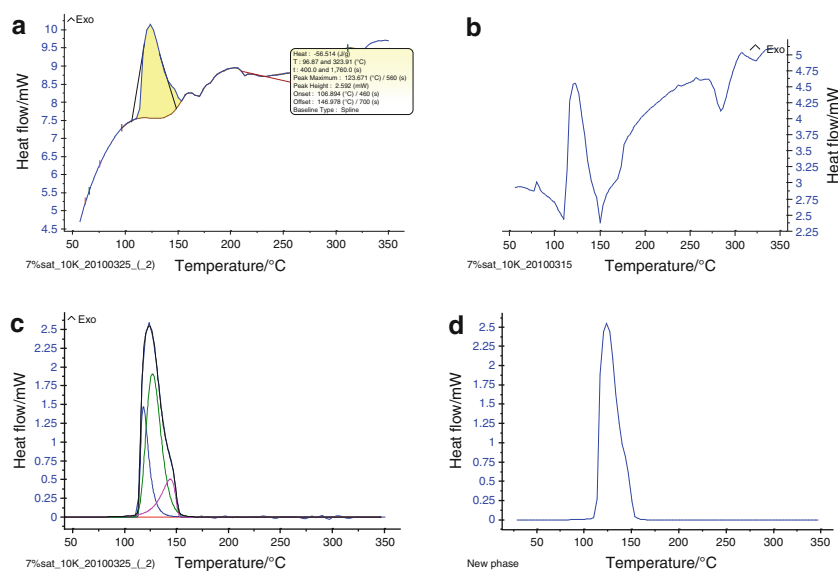
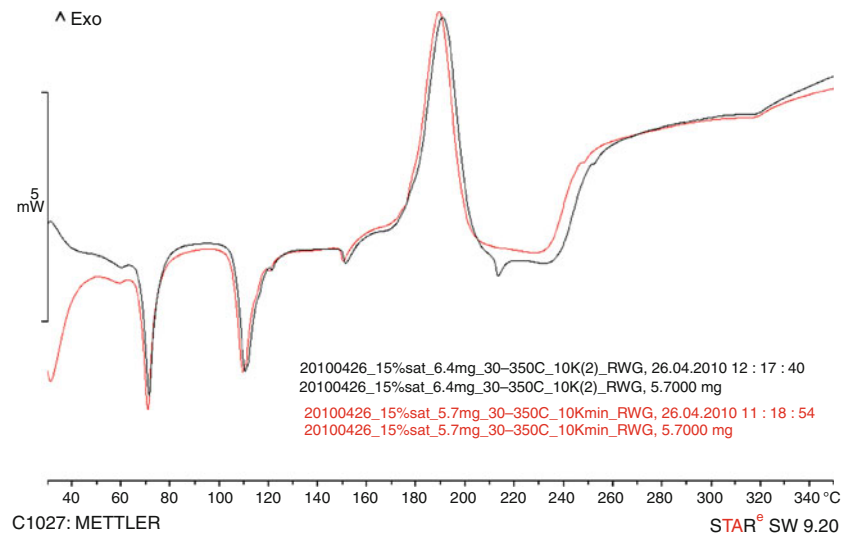
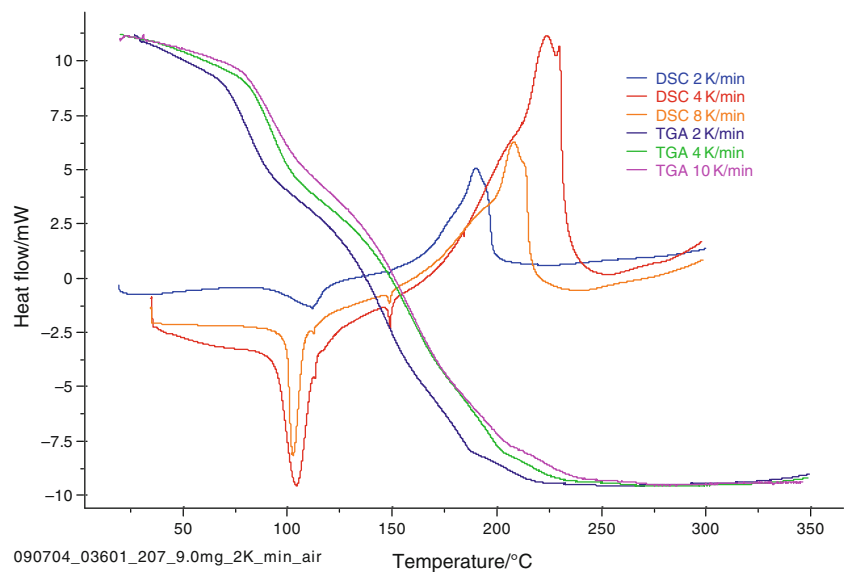


Fig. 2 Reproducibility of sample 03601-207 at 10 K**Fig. 3** Comparison of DSC and TGA curves for sample 03-601 at 207 m**Table 1** Classification of ore samples from Reid Brook deposit

Sample	Borehole	Depth/m	Field observation(s) ^a
1	03-601	199.0	No oxidation noted
2	03-601	207.1	Strongly oxidized
3	03-601	219	Weakly oxidized
4	07-824	476.5	Strongly oxidized
5	07-833	121	Weak oxidation
6	07-840	117	Bronze color
7	05-658	225	No oxidation noted
8	05-658	257	No oxidation noted
9	07-829	200	Slight oxidation
10	07-829	210	Rapid oxidation
11	05-669	192	N/A
12	05-670	198	N/A
13	06-774	352	N/A

^a Observed after logging of samples

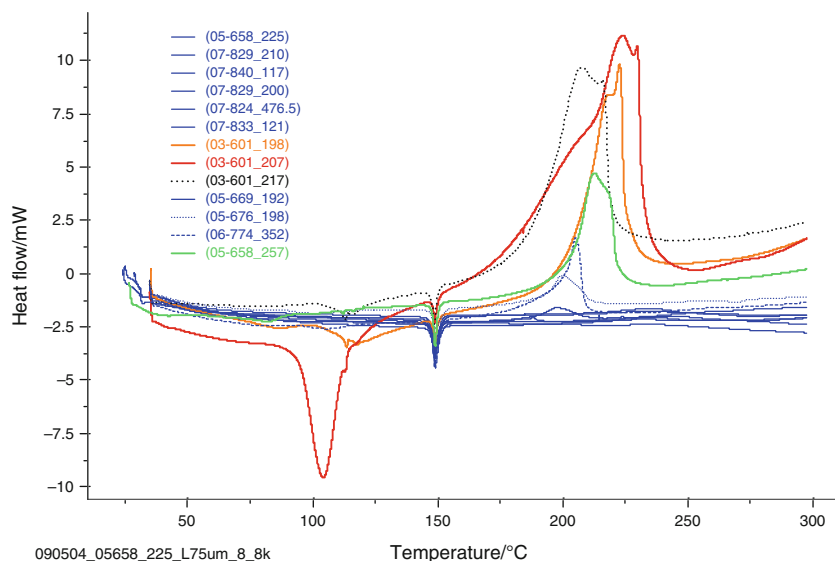
that the ores generally show a similar profile, featuring at least two endothermic peaks in the range of 85–160 °C followed closely by an exothermic peak ranging from 175 to 250 °C. However, except for samples 03-601 at different depths and 05-658 at the depth of 257 m, the other samples do not show significant exotherms. As a result, samples 03-601 (designated sample A–C) and samples 05-658 (Sample D) were selected for investigation of effect of mineralogy. To rule out the effect of particle size and moisture contents, which have been reported to effect self-heating [9, 10], both of these parameters were held constant at <75 μm and 3% moisture saturation respectively.

Reaction rate

Figure 5 shows a comparison of the reaction rates of the sulfide mineral ores, both measured and predicted, after

Table 2 Mineralogy of ore samples from Reid Brook deposit

Borehole	Depth/m	Pyrrh	Troil	Pentla	Chalc + Cuba	Magn	Plagio	Biotite	Chlori	Fayali
03-601	198.6	64.47	–	8.47	19.71	3.07	Nd	0.02	0.02	0.01
03-601	207	73.34	–	6.89	14.03	3.13	Nd	0.04	0.01	Nd
03-601	217.2	84.74	–	6.28	5.6	1.42	Nd	0.04	0.01	Nd
07-824	476.5	71.19	18.13	6.58	2.64	0.45	0.15	0.09	0.10	0.02
07-833	121	67.89	14.04	12.06	4.12	1.76	Nd	0.01	Nd	Nd
07-840	117	55.61	15.95	10.86	6.29	1.21	1.27	1.17	2.19	2.34
05-658	225	68.44	19.03	8.83	2.92	0.78	Nd	Nd	Nd	Nd
05-658	257	49.92	15.62	20.39	13.13	0.87	Nd	Nd	Nd	Nd
07-829	200	74.62	11.50	7.62	2.51	1.92	Nd	0.06	1.23	0.27
07-829	210	68.32	15.02	9.21	5.66	1.53	Nd	0.02	0.01	0.02
05-669	192	53.42	12.29	21.61	10.17	2.24	Nd	Nd	0.00	0.07
05-670	198	59.43	12.52	15.27	10.76	1.72	Nd	Nd	0.00	0.03
06-774	352	57.91	14.57	20.21	4.58	2.44	Nd	0.05	0.00	0.04

Fig. 4 Obtained DSC signals with the ore samples in air at $8\text{ }^{\circ}\text{Cmin}^{-1}$ 

advanced kinetic analysis using AKTS software. The precise prediction of DSC data is evident with overall correlation coefficient greater than 0.99. This clearly shows the versatility of iso-conversional differential method of AKTS for kinetic simulations.

As shown in Fig. 5, samples A–C exhibit significantly larger reaction rate compared to sample D. This can be attributed to the 67% lower pyrrhotite content [6, 11], and a three times larger content of less reactive pentlandite in sample D [7]. It has been reported that pyrrhotite oxidizes rapidly at very low temperatures under atmospheric conditions [12]. It also has an increased surface area for oxidation as fractures extend deeply not only into the sample aggregated clumps but into the individual pyrrhotite grains as well [13]. As could be observed in Table 3, Samples B

and C have a detected onset temperature of 150 °C, possibly due to the lower levels of trace metals i.e., copper and nickel [13].

Another parameter of interest is the sample's Fe/S ratio, which causes larger heat evolution at higher values [13]. This is because a high Fe/S ratio implies increased Fe^{3+} content—a vigorous oxidizing agent results in pronounced oxidation, e.g., for sample B, $\text{Fe/S} = 1.55$ is highest and $\Delta H = 236.3 \pm 48\text{ L J g}^{-1}$ is largest as shown in Tables 4 and 5, respectively. It is also evident from Fig. 5 that sample A has the highest reaction rate, despite its delayed detected onset. This can be attributed to presence chalcopyrite (CuFeS_2)—a mineral known to be very reactive although with relatively high activation energy [6, 14]. This point would be discussed further in subsequent sections.

Fig. 5 Comparison of measured and predicted reaction rates **a** 03-601 [198 m], **b** 03-601 [207 m], **c** 03-601 [217 m], **d** 05-658 [257 m]

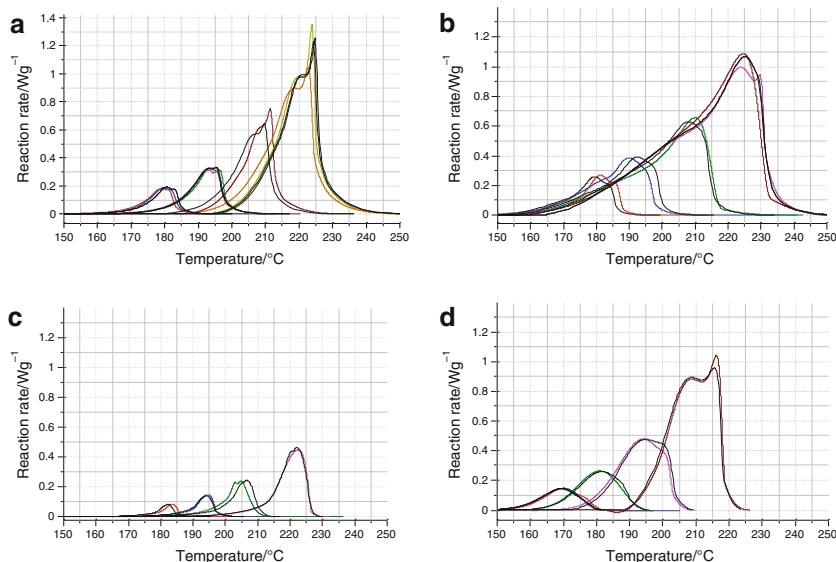


Table 3 Effect of mineralogical ratio on onset temperature

Borehole	Pyrr	Pent	Pyrr/Pent ratio	Fe	S	Fe/S ratio	Trace ^a /wt%	Onset/°C ^b
03-601 (A)	64.47	8.47	7.61	54.40	36.32	1.498	10.57	170
03-601 (B)	73.34	6.89	10.64	56.90	36.72	1.550	5.34	150
03-601 (C)	84.74	6.28	13.51	56.18	37.66	1.492	5.21	150
05-658 (D)	49.92	20.39	2.45	51.41	34.31	1.497	11.85	170

^a Trace metal content found by addition of percent Ni and percent Cu

^b Detected onset temperature

Table 4 Elemental analysis of ore samples from Reid Brook deposit

Sample	Borehole	Depth/m	Fe	S	Ni	Cu	Others/wt%
1	03-601	198.60	54.40	36.32	5.70	4.87	0.00
2	03-601	207.00	56.90	36.72	3.80	1.54	1.04
3	03-601	217.20	56.18	37.66	3.70	1.51	0.96
4	07-824	476.5	50.9	36.1	2.7	0.9	9.4
5	07-833	121	51.8	36.9	3.6	1.4	6.2
6	07-840	117	50.5	33.4	4.1	2.3	9.6
7	05-658	225	56.28	36.40	3.34	1.04	2.95
8	05-658	257	51.41	34.31	7.20	4.65	2.42
9	07-829	200	51.5	34.6	3.3	1.0	9.6
10	07-829	210	51.8	36.2	3.5	1.9	6.6
11	05-669	192	53.38	34.94	6.46	3.69	1.56
12	05-670	198	54.52	34.06	3.27	2.06	6.08
13	06-774	352	54.59	33.54	3.48	1.13	7.26

Apparent activation energy

Using the Friedman's differential iso-conversional method, the dependence of apparent activation energy on reaction progress was estimated as shown in Fig. 6. The resulting correlation coefficient was greater than 0.99 in all cases

supporting the accuracy of estimates. A common observable trend in Fig. 6 is the high initial apparent activation energy, followed by a downward slope with a sharp rise between α of 0.7–0.9. Sample D, with the lowest pyrrhotite/pentlandite ratio, has the highest overall apparent activation energy as per ASTM method (Table 5). However, the Friedman analysis shows a sharp rise in the apparent activation energy toward the end of the reaction. For sample D, it appears that the larger content of the less reactive pentlandite constitutes a barrier to the sample's oxidation especially as the reaction progresses toward completion. This explanation is supported by a prior finding that oxidation of pentlandite-rich causes thickening of oxide layers, which inhibits oxygen diffusion, resulting in sharp increase of apparent activation energy toward end of reaction [15]. In contrast, for the pyrrhotite-rich ores (i.e., samples A–C) the observed mild increase in apparent activation energy toward the end of the reaction is attributable to the formation of a weaker mantle due to lower pentlandite levels, which reduces the inhibition of gas diffusion critical to the reaction [14, 15]. As per the ASTM method, the pyrrhotite-rich samples (A–C) exhibit larger and comparable apparent activation (average $E_A = 77 \text{ kJ mol}^{-1}$) with the highest being for sample C

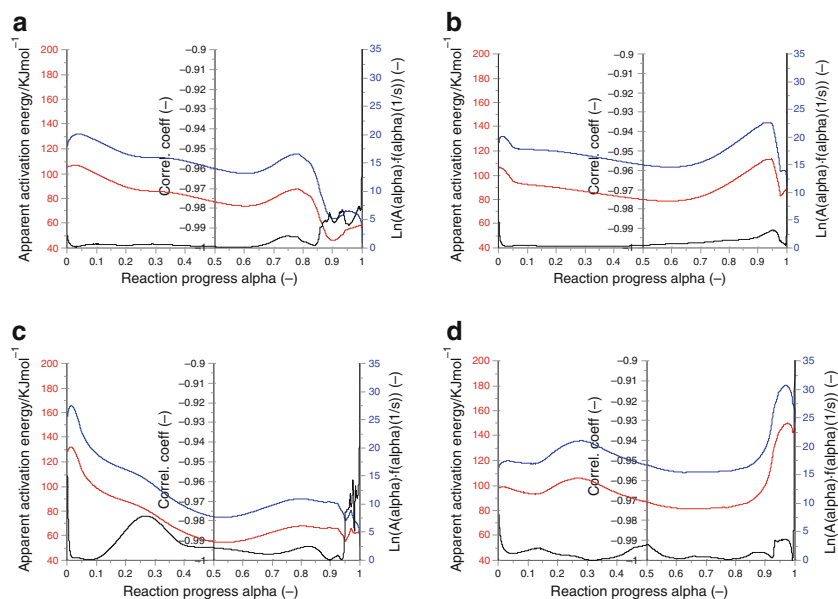
Table 5 Effect of mineralogy on thermo-kinetic parameters of ore samples

Sample	$\Delta H_r/Jg^{-1}$	$E_A/k J mol^{-1}$ [Friedman]	$E_A/k J mol^{-1}$ [ASTM E698]	dTAD/ $^{\circ}C$ ($\phi = 1/\phi = 2$)	TMR/ $^{\circ}C$	SADT/ $^{\circ}C$
A	-119.8 ± 12.3	40-100	78.585	199/99	104.53	72
B	-236.3 ± 48.1	50-135	77.822	393/196	115.34	81
C	-126.8 ± 39.4	80-110	75.123	211/105	94.17	63
D	-35.8 ± 6.3	80-150	92.939	50.5/25.2	108.73	72

A 03-601 [198 m], B 03-601 [207 m], C 03-601 [217 m], D 05-658 [257 m]

Fig. 6 Apparent activation energy against reaction progress

a 03-601 [198 m], **b** 03-601 [207 m], **c** 03-601 [217 m], **d** 05-658 [257 m]



($E_A = 75 k J mol^{-1}$) owing to its higher pyrrhotite/pentlandite ratio (≈ 13.5 see Table 3). Since the Fe/S ratios of samples A, C, and D are relatively close, it appears that the prime factors governing their estimated apparent activation energy is the pyrrhotite and pentlandite content rather than Fe/S ratio or trace metal content. Nonetheless, further testing on the effect of troilite (found in sample D but absent in others) would need to be investigated for a more complete understanding of mineralogy effects on the sample's self-heating.

Self-heating diagrams

Figure 7 displays the self-heating diagrams of the four samples at a base process temperature of $100^{\circ}C$ in terms of reaction rate and reaction progress versus time. It is evident that all the samples achieve runaway status at different times. Samples A and C run away the quickest in less than 2 days! The behavior of the apparent activation energy profile is also mirrored in the self-heating plots shown in Fig. 7, especially for Φ values between 1 and 2. On the other hand, sample B attained the longest runaway status owing to its high initial apparent activation energy.

Thus, it can be inferred that similarity in apparent activation energy profiles of samples A and D results in both sample's comparable runaway status; a behavior that could be attributed to the comparable trace metal contents.

As shown in Table 5, sample D has the lowest T_{AD} (adiabatic temperature rise), due to the lowest pyrrhotite levels, whereas samples B and C have a high T_{AD} , a consequence of the higher Fe/S ratio, higher pyrrhotite/pentlandite ratio, and lower trace metal content. Moreover, sample B has a higher T_{AD} than sample A due to the higher Fe/S ratio. Sample A and D show a lower T_{AD} , mirrored by the increased levels of trace metal content and decreased levels of pyrrhotite.

Safety diagram and time to maximum rate (TMR)

Figure 8 displays the TMR and safety diagrams of the four samples. The labeled temperature corresponds to the temperature at which in 24 h the reaction will run away. Consistent with previous results, sample C exhibit the lowest temperature at TMR of $94.17^{\circ}C$ attributable to the combined effect of a high pyrrhotite/pentlandite and low Fe/S ratios [6]. As reported by [15]; higher levels of sulfur

Fig. 7 Predicted self-heating diagrams **a** 03-601 [198 m], **b** 03-601 [207 m], **c** 03-601 [217 m], **d** 05-658 [257 m]

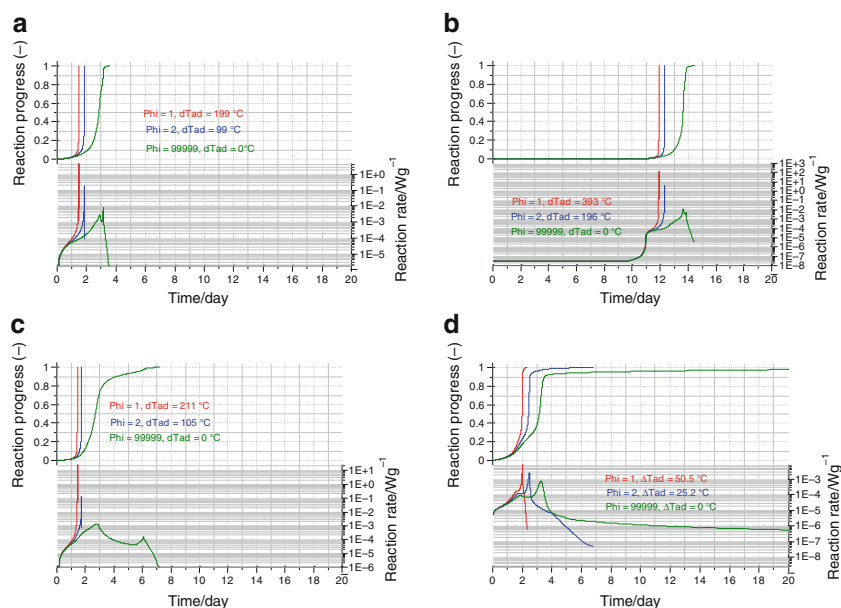
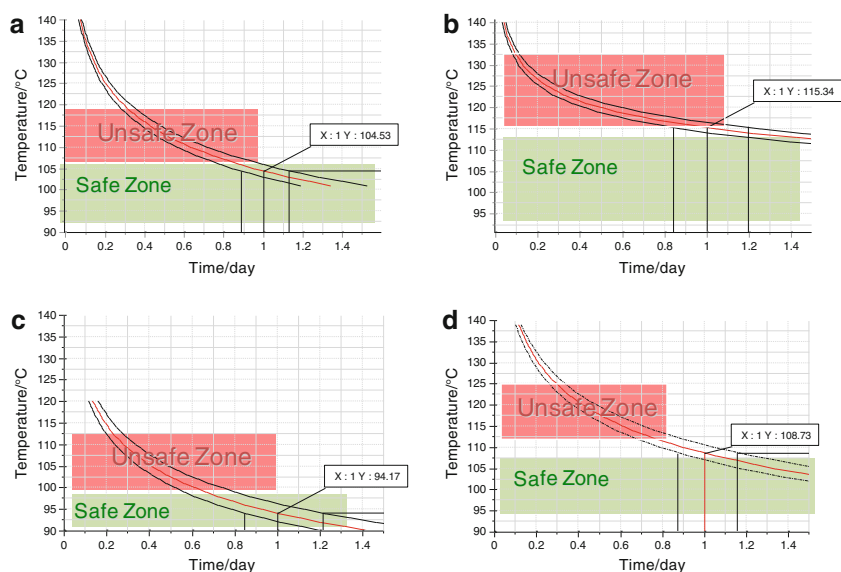


Fig. 8 Predicted safety diagrams **a** 03-601 [198 m], **b** 03-601 [207 m], **c** 03-601 [217 m], **d** 05-658 [257 m]



lower the decomposition temperature of sulfide mineral ores. Samples A and D exhibit a temperature of 104 and 107 °C to TMR respectively, owing to the high copper content. Conversely, sample B has the highest temperature to TMR, due to the high apparent activation energy to self-heating as discussed earlier. Therefore, these results suggest that high copper content causes lower temperature to TMR because of accelerated reaction rate of copper despite exhibiting higher apparent activation energy initially.

Self-accelerating decomposition temperature (SADT)

SADT is the lowest ambient temperature at which sample's interior overheats by over 6 °C after an elapse of at least 7 days. This temperature and associated profile is shown in

Fig. 9. As expected, sample C has the lowest SADT of 63 °C—a consequence of combination of factors, such as high pyrrhotite/pentlandite ratio, high iron/sulfur ratio, low trace metal content as previously explained. Samples A and D having comparable amounts of the trace metals and Fe/S ratios showed similar SADT values of 72 °C. However, the estimated SADT value of Sample B is unexpectedly high (i.e., 81 °C), which is surprising since the sample exhibits relatively comparable pyrrhotite/pentlandite ratio, and trace metal contents to Sample C. A plausible explanation could be that higher Fe/S ratio of sample B results in the uncharacteristically larger initial E_A (see Fig. 6) having adverse effect on its SADT value. However, further study would be required to validate this explanation. Thus, a preliminary inference from this result is that Fe/S ratio has

Fig. 9 Predicted SADT diagrams **a** 03-601 [198 m], **b** 03-601 [207 m], **c** 03-601 [217 m], **d** 05-658 [257 m]

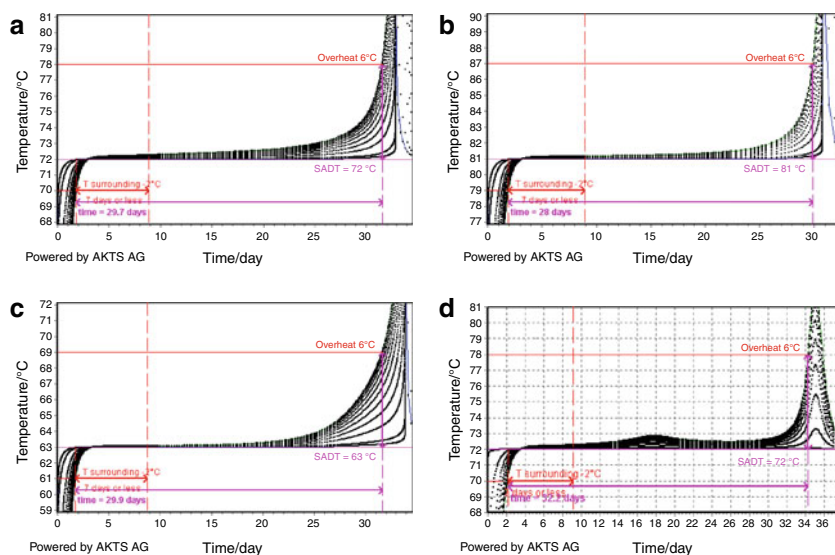
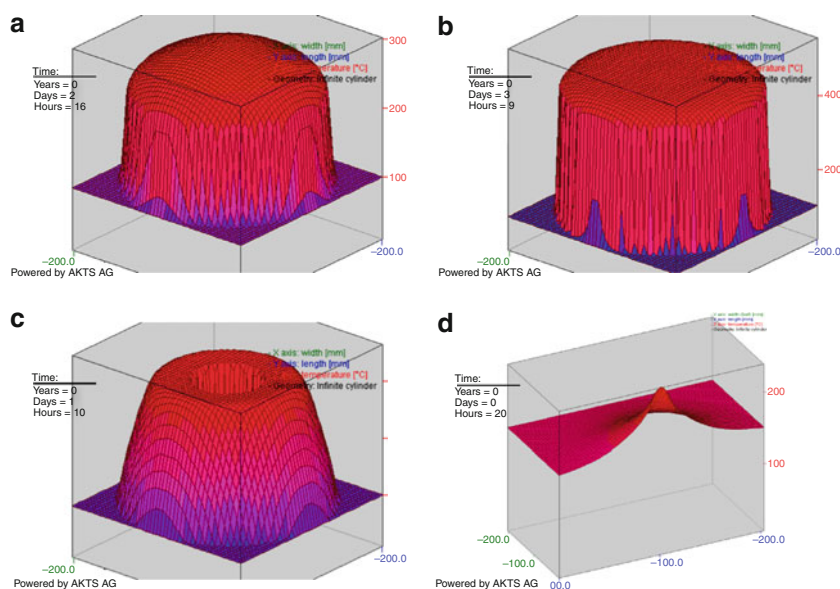


Fig. 10 Predicted 3-D simulation **a** 03-601 [198 m], **b** 03-601 [207 m], **c** 03-601 [217 m], **d** 05-658 [257 m]



a critical role to play in the sample's self-accelerating decomposition temperature. However, the specific nature of the relationship between self-heating and SADT needs to be further investigated.

Three-dimensional simulation

The AKTS software not only predicts the self-heating tendency of the sample, but is also able to project a 3D-simulated timeline of the self-heating behavior. Figure 10 shows the 3D simulation depicting sample's temperature history and profile from the container exterior to the interior. It is evident that high levels of pyrrhotite cause a rapid runaway reaction at the exterior of the container, whilst the interior remains shielded (e.g., as observed in Fig. 9b and c

but absent in Fig. 9a). Abundant sulfur reacts with O_2 at the surface, raising the temperature on the exterior and speeding up oxidation of iron; an exothermic process that causes spiking at the exterior [15]. Also, during the reaction, there is a diffusion of Ni and Fe atoms from the pyrrhotite to the exterior [12]. The other samples with higher pentlandite have a greater tendency to form a protective coating or a rim on the exterior, inhibiting gas diffusion and reaction on the exterior as shown in Figs. 9a and d [15, 16]. Thus, a higher pyrrhotite/pentlandite ratio will have a quicker reaction, and may also have a spiking at the exterior of the cell. Also, samples A and D have a higher trace metal content and thereby a higher onset temperature; thereby oxidizing slower [13] which allows thorough heat transfer. High pentlandite levels in sample D

cause thickening of oxide layers, which inhibits diffusion of oxygen, and increases activation energy toward end of reaction [15]. A lower trace metal content for B and C allows a quicker onset temperature and faster oxidation. However, Samples A and B with a high level of chalcopyrite allow thorough heat transfer throughout the samples, permitting a broad rounded top 3-D profile.

Conclusions

The primary mineralogical variables influencing self-heating of sulfide ores are primarily pyrrhotite, pentlandite, and chalcopyrite; as well as pyrrhotite/pentlandite ratio, iron/sulfur ratio, and trace metal content. An increase in pyrrhotite level, or pyrrhotite/pentlandite ratio, causes a more vigorous reaction with a higher reaction rate and thus a lower TMR and SADT, as pyrrhotite oxidizes rapidly under atmospheric conditions and has a greatly increased surface area. Pentlandite's oxidation mantle greatly inhibits the reaction via a decrease in gas diffusion, whereas pyrrhotite's oxidation mantle can be nullified due to the high surface area. The higher the pyrrhotite content, the higher the self-heating propensity and larger the exothermic release at the exterior of the sample. Pentlandite however shows a more thorough heating of the ore sample. An increase in trace metal content, primarily copper and nickel, causes an increase in the onset temperature of the reaction; affecting the TMR but has a negligible effect on the SADT. Chalcopyrite, rich in copper, exhibits higher apparent activation energy, causing interior self-heating. While it does accelerate self-heating behavior, it tends to have higher apparent activation energy, limiting the overall effect of self-heating. It also causes an overall rounded 3D shape as the higher activation energy allows a thorough heat transfer throughout the sulfide ore. An increase in Fe/S ratio causes a higher heat evolution. An overall increase in sulfur levels decreases ignition temperature of pyrrhotite, thereby decreasing the TMR and SADT.

Acknowledgements The authors wish to thank Mr. Alex Dias for running all the AKTS simulations and valuable technical discussions.

We like to acknowledge Mr. Ryan Gillespie for conducting some of the DSC/TGA tests. We also wish to thank Dr. Lawrence Cochrane for his revision and valuable comments on this paper, and Vale Inco for supplying samples and providing financial support.

References

1. Iliyas A, Hawboldt K, Khan F. Thermal stability investigation of sulfide minerals in DSC. *J Hazard Mater.* 2010;178:814–22.
2. Iliyas A, Hawboldt K, Khan F. Advanced kinetics for calorimetric techniques and thermal stability screening of sulfide minerals. *Thermochim Acta.* 2010;501:35–45.
3. Zamalloa M, Utigard TA. The behaviour of Ni-Cu concentrate in an industrial fluid bed roaster. *Can Metall Quart.* 1996;35:435–49.
4. Zivkovic ZD, Mitevska N, Savovic V. Kinetics and mechanism of the chalcopyrite-pyrite concentrate oxidation process. *Thermochim Acta.* 1996;283:121–30.
5. Dunn JG, Mackey LC. The measurement of ignition temperatures and extents of reaction on iron and iron-nickel sulfides. *J Therm Anal.* 1991;37:2143–64.
6. Rosenblum F, Nessel J, Spira R. Evaluation and control of self-heating in sulphide concentrates. *Cim Bull.* 2001;94:92–9.
7. Dunn JG. The oxidation of sulphide minerals. *Thermochim Acta.* 1997;300:127–39.
8. Rosenblum F, Spira P. Evaluation of hazard from self-heating of sulfide rock. *Cim Bull.* 1995;88:44–9.
9. Dunn JG, De GC, Oconnor BH. The effect of experimental-variables on the mechanism of the oxidation of pyrite.1. Oxidation of particles less than 45-Mu-M in size. *Thermochim Acta.* 1989;145:115–30.
10. Jerz JK, Rimstidt JD. Pyrite oxidation in moist air. *Geochim Cosmochim Acta.* 2004;68:701–14.
11. Belzile N, Chen YW, Cai MF, Li YR. A review on pyrrhotite oxidation. *J Geochem Explor.* 2004;84:65–76.
12. Wang HP. A review on process-related characteristics of pyrrhotite. *Miner Process Extr Metall Rev.* 2008;29:1–41.
13. Janzen MP, Nicholson RV, Scharer JM. Pyrrhotite reaction kinetics: reaction rates for oxidation by oxygen, ferric iron, and for nonoxidative dissolution. *Geochim Cosmochim Acta.* 2000;64:1511–22.
14. Dutrizac JE. Reactions in cubanite and chalcopyrite. *Can Mineral.* 1976;14:172–81.
15. Wang HP, Pring A, Xie YN, Ngothai Y, O'neill B. Phase evolution and kinetics of the oxidation of monosulfide solid solution under isothermal conditions. *Thermochim Acta.* 2005;427:13–25.
16. Dunn JG, Kelly CE. A TG-MS and DTA study of the oxidation of pentlandite. *J Therm Anal.* 1980;18:147–54.